

Manganese-Enhanced MRI: An Exceptional Tool in Translational Neuroimaging

Afonso C. Silva^{1,2} and Nicholas A. Bock²

²Cerebral Microcirculation Unit, Laboratory of Functional and Molecular Imaging, National Institute of Neurological Disorders and Stroke, National Institutes of Health, Bethesda, MD 20892, USA

The metal manganese is a potent magnetic resonance imaging (MRI) contrast agent that is essential in cell biology. Manganese-enhanced magnetic resonance imaging (MEMRI) is providing unique information in an ever-growing number of applications aimed at understanding the anatomy, the integration, and the function of neural circuits both in normal brain physiology as well as in translational models of brain disease. A major drawback to the use of manganese as a contrast agent, however, is its cellular toxicity. Therefore, paramount to the successful application of MEMRI is the ability to deliver Mn²⁺ to the site of interest using as low a dose as possible while preserving detectability by MRI. In the present work, the different approaches to MEMRI in translational neuroimaging are reviewed and challenges for future identified from a practical standpoint.

Key words: manganese/magnetic resonance imaging/animal models/brain/contrast agents/brain function/neuronal tracts/brain disease

Introduction

The ability of magnetic resonance imaging (MRI) to provide high spatial resolution images with exquisite soft tissue contrast noninvasively has led to great efforts in the development of contrast agents that add physiological, biochemical, and molecular information to the detailed anatomical information provided already available.¹ A particularly useful contrast agent for imaging the brain is the metal manganese, in the form of its divalent ion,

Mn²⁺, which is paramagnetic and causes strong reduction of both T₁ and T₂ relaxation time constants of tissue water. Manganese is an essential heavy metal that is an important cofactor in a number of key enzymes, including manganese superoxide dismutase,^{2,3} pyruvate carboxylase,⁴ and glutamine synthetase.⁵ Indeed, complex mechanisms of nutritional absorption, transport in blood, and brain uptake are in place to maintain levels of manganese at physiologically stable levels,^{6–8} and many of those mechanisms are just beginning to be understood at a molecular level.^{6,8,9} In the central nervous system (CNS), Mn²⁺ can enter excitable cells via some of the transport mechanisms for calcium (Ca²⁺),⁶ including voltage-gated Ca²⁺ channels, the sodium (Na⁺)/Ca²⁺ exchanger, the Na⁺/magnesium (Mg²⁺) antiporter, and the active Ca²⁺ uniporter in mitochondria.¹⁰ In addition, Mn²⁺ can bind intracellularly due to its affinity for Ca²⁺ and Mg²⁺ binding sites on proteins and nucleic acids. Once inside cells, some Mn²⁺ is transported anterogradely in axonal tracts.^{11,12} Upon reaching the presynaptic membrane, it is released into the synaptic cleft along with the neurotransmitter glutamate,¹³ suggesting that Mn²⁺ may influence synaptic transmission in the brain.¹⁴

Taken together, the above mentioned properties of manganese make it a particularly attractive contrast agent for MRI of the brain, and 3 major classes of applications of manganese-enhanced magnetic resonance imaging (MEMRI) have materialized:^{15–18} First, systemic administration of Mn²⁺ has opened up new MRI-based strategies for enhancement of the cerebral neuroarchitecture, leading to unique MRI enhancement in specific areas of the brain.^{19–26} Second, Mn²⁺ will move along appropriate neuronal pathways in an anterograde fashion when injected to specific brain regions, allowing MEMRI to map neuronal tracts in the living brain.^{27–38} Third, due to the ability of Mn²⁺ to enter excitable cells through voltage-gated calcium channels, MEMRI can be used to demarcate active regions of the brain, providing an attractive means to probe cerebral function with a hemodynamic-independent contrast.^{39–47} Work in these 3 areas has led to an emergence of MEMRI to study translational models of cerebral disease based on the unique properties of Mn²⁺ as a contrast agent.

¹To whom correspondence should be addressed: Cerebral Microcirculation Unit, Laboratory of Functional and Molecular Imaging, National Institute of Neurological Disorders and Stroke, National Institutes of Health, 10 Center Drive MSC1065, Building 10, Room BID106, Bethesda, MD 20892-1065; tel: 301-402-9703, fax: 301-480-2558, e-mail: silvaa@ninds.nih.gov

Administration of MnCl₂ for MEMRI: How Much is Too Much?

Key to the successful application of MEMRI for the major classes of experiments mentioned above is the ability to deliver Mn²⁺ to the site of interest at an appropriate dose and in a timely manner. However, while Mn²⁺ in trace amounts is an essential ion for normal development and cellular function, overexposure to the metal leads to a progressive and permanent neurodegenerative disorder in humans and nonhuman primates called manganism, which resembles Parkinsonism in its symptoms.^{48,49} Patients develop signs that include generalized bradykinesia, widespread rigidity, and occasional resting tremor that are related to damage to the basal ganglia caused by substantial regional accumulation of manganese.⁴⁸ In addition to the deleterious effects of chronic overexposure, acute overexposure to Mn²⁺ (as when a systemic dose of the contrast agent is administered) can also lead to hepatic failure⁵⁰ and cardiac toxicity.⁵¹ Nevertheless, because magnetic resonance relaxation rates are proportional to the effective concentration of Mn²⁺ in tissue, significant amounts of Mn²⁺ are required to produce robust and detectable MRI contrast. This means that a compromise exists between avoiding toxicity and delivering adequate amounts of manganese for MEMRI.

For systemic injections targeting the whole brain, the simplest way to deliver Mn²⁺ is to inject a solution of the salt MnCl₂ intravenously, intraperitoneally, or subcutaneously. The solution can be made in distilled water but should be buffered to a biological pH and corrected for osmolarity.⁵² There has been little work studying whether different salts of Mn²⁺ significantly alter the detected contrast, although any salt that readily produces free Mn²⁺ in biologically compatible solutions should be adequate. One study investigated the relative MRI enhancement obtained with different routes of administration and concluded that both the temporal and regional changes in cerebral T₁ following MnCl₂ infusion are relatively independent of the route of administration.⁵³ The material safety data sheet for MnCl₂ shows that doses as low as 93 mg/kg for rats or 38 mg/kg for mice have significant adverse effects and mortality rates.⁵² However, current MEMRI experiments have been safely performed at similar doses, or even higher, with good results and manageable adverse effects. When using systemic administration, we have been able to reliably infuse as much as 175 mg/kg intravenously in healthy rats up to 250 g body weight,²² and in mice up to 25 g body weight.⁵⁴ On the other hand, it is unlikely that animal models of brain diseases will tolerate such a dose. In addition, such high doses are not advisable for longitudinal studies in which repeated injections and imaging sessions are required. Furthermore, it is unlikely that the above doses scale across different species. Therefore, optimization of the

dose of manganese to be administered needs to be carefully performed prior to carrying out fully fledged studies.

Recently, we devised a methodology that consists of administering small fractionated injections of manganese over time to build detectable doses in the brain while lessening the effects of acute exposure to other organs.²⁴ Our methodology is based on the long half-life of manganese in the brain (51–74 days)⁵⁵ relative to its short half-life in visceral organs like the heart and the liver. Based on a toxicology study that reported a good tolerance in rats to daily systemic injections of 30 mg/kg MnCl₂,⁵⁶ we demonstrated significant enhancement followed by saturation of the MEMRI signal in most regions of the brain, except the cortex, after 6 fractionated doses of 30 mg/kg administered every 48 h (figure 1).²⁴ This fractionation method was well tolerated by the rats even after 12 injections.²⁴ We also showed that signal enhancement increased with the dose of the individual fractions and concluded that the amount of manganese that ultimately accumulates in the brain parenchyma depends on the concentration gradient of manganese between the blood and the brain tissue.²⁴ Higher fractional doses deliver more manganese to tissue at each application, but the accumulation of manganese in the parenchyma with each dose reduces the driving gradient, causing eventual saturation of signal enhancement. Because systemic toxic effects become worse at higher fraction doses of manganese, researchers planning MEMRI studies should first find the highest fraction dose that the animals will tolerate health-wise and then determine the number of fractionated injections needed to fully enhance the signal.

The issue of toxicity is less severe in MEMRI experiments that use local injections of MnCl₂ in the brain because there is little exposure to Mn²⁺ outside of the injection site and immediately adjacent areas. A range of studies have used direct injections of small volumes (10–1000 nl) of MnCl₂ in different concentrations (5 mM–2.48 M) to trace neuronal connections in the brain of rodents,^{27–29} birds,³⁰ monkeys,^{31,36} and the minipig.⁵⁷ However, the local toxicity of the injections may still need to be considered, depending on the application. A recent study tracing sensorimotor connections in the rat brain reported that acute injections of 100 mM MnCl₂ solutions in brain parenchyma cause glial reaction for manganese loads above 8 nmol and neuronal cell death for loads at or above 16 nmol.³⁸ Notwithstanding, the same study demonstrated that much larger amounts of Mn²⁺ could be delivered into brain tissue with negligible toxic effects by continuous infusion of low concentrations of MnCl₂, suggesting that under such conditions Mn²⁺ is continuously transported away from the injection site by neurons and detoxified by glial cells, both factors contributing to prevent the tissue concentration to reach the toxic threshold.³⁸

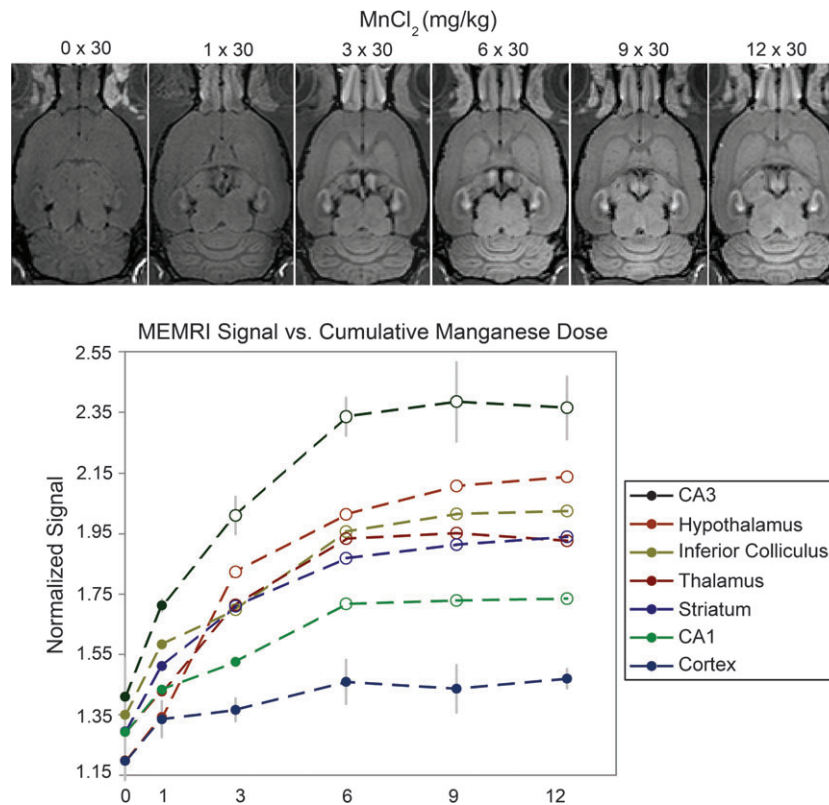


Fig. 1. Effect of increasing numbers of fractions of MnCl_2 on the signal intensity in MEMRI of the rat brain. The top row shows typical horizontal slices from 3D T_1 -weighted images of a rat at increasing cumulative doses of 30 mg/kg MnCl_2 delivered systemically at 48-h intervals between doses. The bottom graph shows the signal magnitude from each brain region normalized to the signal intensity in the temporalis muscle (error bars = ± 1 SD, $n = 4$). Progressive signal enhancement is observed in most regions of the brain, except the cortex, with the number of fractions, up to 6 fractions, after which saturation of the MEMRI signal intensity is reached. Open data points denote significantly higher signal intensity in manganese-injected rats compared with controls ($P < .05$).

MEMRI of the Neuroarchitecture

Unlike chelated gadolinium contrast agents, which remain in the cerebral vasculature, the MRI contrast obtained after a systemic administration of MnCl_2 comes from the brain tissue itself. Since Mn^{2+} enhances brain regions according to their propensity to uptake the metal, it has been very useful for visualizing the brain architecture. Indeed, recent works in rodents,^{19–23,25,54, 58} non-human primates,²⁶ and insects⁵⁹ have demonstrated the usefulness of manganese to provide cytoarchitectonic contrast of the brain. For example, figure 2A shows a horizontal view of a rat brain 24 h after a systemic intravenous injection of 180 mg/kg MnCl_2 . A superb contrast enhancement of the brain cytoarchitecture was obtained due to the increased presence of Mn^{2+} in regions such as hippocampus (Hip), habenula (Hab), colliculi (Col), cerebellum (CEB), and olfactory bulb (OB). This pattern of contrast enhancement can be obtained over a wide range of systemic doses,⁵⁴ with regions of the brain which lack a blood-brain barrier (BBB), such as the pituitary gland (Pit) and the pineal gland (Pi) showing strong enhancement at doses as small as 9 mg/kg, and regions of intact BBB, such as the Hip, CEB, and cortex showing a dose-

dependent increase in contrast enhancement. Indeed, there is even MEMRI contrast variation in the cortical laminae, the highest signal intensity coinciding with the histological locations of mid-layer II and the transition zone from mid-layers IV to V.²⁵ Such detailed contrast can even be used to characterize mutant mice; laminar contrast is not present in the reeler mutant mouse,²⁵ which is known to have a disorganized cortical structure, but is enhanced in the bassoon mutant mouse,⁶⁰ which is known to have increased cortical volume and thickness. However, these finer details of the neuroarchitecture, as shown in figure 2A (arrows), can only be detected with high-resolution MRI at higher doses such as 90 or 180 mg/kg.^{22,25,54}

The pattern of signal enhancement in the brain following administration of manganese originates in the ventricles and moves to periventricular regions prior to reaching more distant regions of the brain parenchyma,^{22,26,54} suggesting that, at the doses used in MEMRI, Mn^{2+} crosses the blood-CSF barrier via the choroid plexus. This is in close agreement with observations of a faster transport system for Mn^{2+} into brain via the choroid plexus, which is 100 times faster than via the blood-brain barrier.^{61,62} In addition, the pattern of regional enhancement is also related to the developmental age of the CNS.^{63,64}

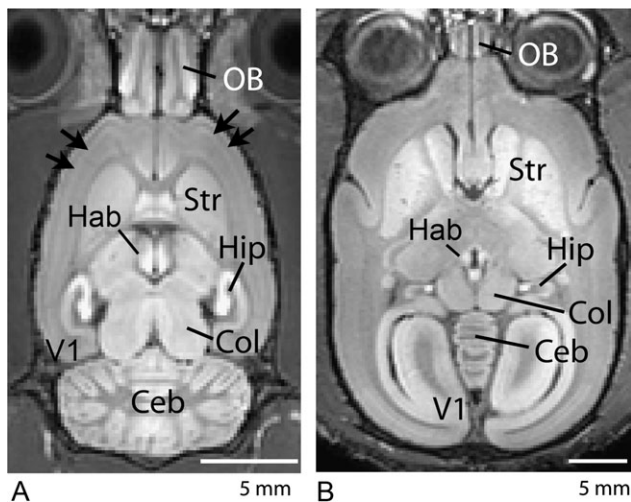


Fig. 2. Typical horizontal T_1 -weighted MEMRI of a rat (A) and a marmoset (B) obtained 48 h after systemic administration of $MnCl_2$. The rat received a single 180 mg/kg $MnCl_2$ injection, while the marmoset received 4 fractionated injections of 30 mg/kg $MnCl_2$ in 48-h intervals. Excellent cytoarchitectonic contrast due to the presence of Mn^{2+} in regions such as the hippocampus (Hip), habenula (Hab), colliculus (Col), cerebellum (CEB), and olfactory bulb (OB). The high dose of administration in the rat allows Mn^{2+} to reveal layers in the OB and in the cortex of the rat (panel A, arrows). In the marmoset (panel B), strong enhancement is observed in the striatum (Str), which is consistent with similar patterns of T_1 -weighted MRI enhancement in human patients after chronic overexposure to manganese. Strong enhancement occurs in the primate visual cortex (panel B, V1) that is not observed in the rat.

Not all species will show the same pattern of regional brain enhancement due to manganese. We recently determined that the pattern of enhancement in the brain of a new-world nonhuman primate, the marmoset (*Callithrix jacchus*), is significantly different than the rodent pattern of enhancement.²⁶ Figure 2B shows a typical horizontal view of the marmoset brain after 4 intravenous injections of 30 mg/kg $MnCl_2$. Not only is there greater signal enhancement in the marmoset brain compared with enhancement in the rat brain after the same manganese administration regimen (see Figs. 1–3 and Table 1 in Bock et al.),²⁶ but also the pattern of enhancement is significantly different from the rat. This is in spite of both species showing the same longitudinal relaxivity for manganese in the brain, which suggests marmosets have a higher brain uptake of manganese from the bloodstream or that the hepatobiliary clearance of manganese from the bloodstream is slower in marmosets so that more manganese is ultimately available for uptake. In addition to showing contrast enhancement in the same brain regions that showed significant enhancement in the rat, the marmoset presents additional enhancement in the basal ganglia, such as the striatum (Str), and also in the thalamus and the visual cortex (V1)—regions that do not enhance significantly in the rat with the same fractionation regimen. Interestingly, 3 of the marmoset

brain regions that showed significantly greater manganese enhancement relative to the rat are located next to large volumes of CSF. The primate visual cortex is adjacent to the posterior horn of the lateral ventricle. In the rat, the posterior horn does not extend to this structure. As well, the caudate of the striatum in the marmoset forms the lateral wall of the anterior horn and body of the lateral ventricle, while the thalamus is bathed anteriorly by the third ventricle. While the same is true in the rat, the CSF space is much smaller than in the marmoset, suggesting that the stronger manganese uptake in the marmoset brain is because of the geometry of the lateral ventricles and third ventricle.

The finding that the marmoset shows significant enhancement of the basal ganglia is consistent with similar patterns of T_1 -weighted MRI enhancement in human patients suffering of chronic overexposure to manganese.⁶⁵ The marmoset also presented strong enhancement in the DG and CA3 subregions of the hippocampus and in the visual cortex, which are regions that could also be involved in manganese-induced neurotoxicity, because not all the neurological symptoms of manganese in humans are explained by damage to the basal ganglia.⁹

MEMRI of Neuronal Tracts

The fact that Mn^{2+} moves along established neuronal pathways is a very useful property for MEMRI applications. The first MEMRI neuronal tracing studies were in the mouse olfactory and visual pathway.²⁷ In the olfactory pathway, MRI enhancement is seen following topical injection of $MnCl_2$ in the nostrils that moves from the turbinates to the olfactory bulb and out of the bulb to the primary olfactory cortex, indicating that Mn^{2+} crosses synapses in addition to being transported along neurons. In the eye, after intravitreal injections of the manganese solution, MRI enhancement moves down the optic nerve and then into the brain, where enhancement of the optical tract and superior colliculus can be detected.²⁷ Similar results have been obtained in the rat^{28,66,67} and in macaques.³⁶ While the earlier studies did not provide evidence of transsynaptic transport in the visual system,^{27,28} the more recent results indicate that the transport of Mn^{2+} in the visual pathway is able to cross synapses and reach the contralateral visual cortex.^{36,66,67} As well, MEMRI following direct injections of $MnCl_2$ in several regions of the brain has been unanimously successful in detecting transport over multiple synapses in neuronal pathways in several species.^{30–33,38,68,69}

One of the most exciting applications of MEMRI of neuronal tracts has been in the study of the changes in size and connectivity of different brain regions due to complex brain processes associated with learning and plasticity. For example, in songbirds, manganese can be used to trace the neuronal tracts connecting the different song control nuclei.^{30,70} Figure 3 shows a schematic

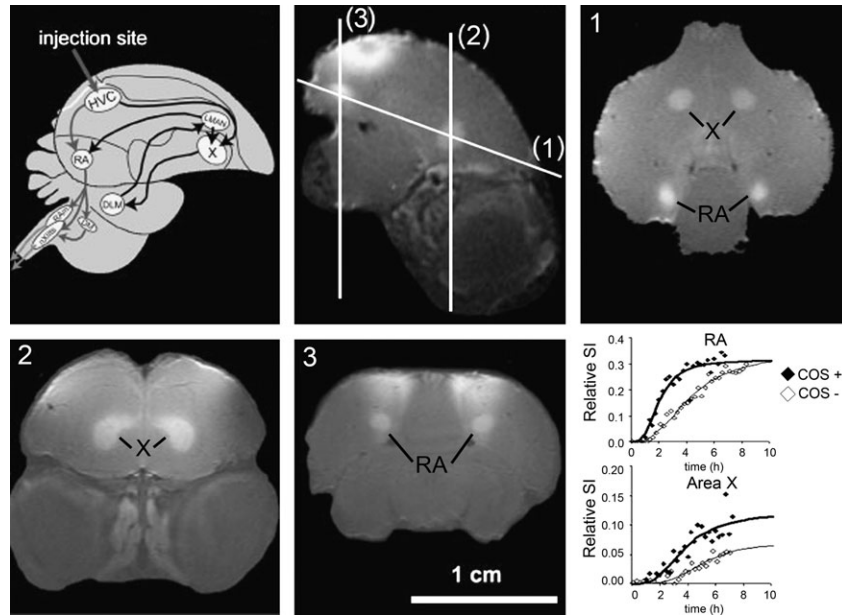


Fig. 3. Schematic overview of the adult songbird brain showing the song control nuclei (SCN) and their connections in the telencephalon (top row, left panel). The black arrows represent the anterior forebrain pathway, which originates from the high vocal center (HVC) to area X, while the gray arrows represent the motor pathway, which originates in distinct cell populations within the HVC that project to the nucleus robustus archistriatalis (RA). Sagittal in vivo MEMRI of a male starling brain obtained 6 h after MnCl_2 injection into the HVC (top row, middle panel). The injection area is indicated by the gray arrow in the left panel and by the enhanced superficial area on the MEMRI. The lines indicate the different planes of imaging labeled (1), (2), and (3), which are displayed on the right panel in the top row and on the left and middle panels of the bottom row, respectively. The areas enhanced by Mn^{2+} are indicated in the MEMRI images. Adapted with permission of A. Van der Linden et al.³⁰ Bottom row, right panel: Changes in the MEMRI relative signal intensity within the 2 song control nuclei (RA and area X) are plotted as a function of time and fitted by nonlinear regression to a sigmoid curve to describe the kinetics of Mn^{2+} accumulation in the RA (top graph) and in area X (bottom graph) and reflects the activity of the respective HVC neuron type. A faster uptake of Mn^{2+} was observed in both areas when the canary was allowed to listen to conspecific canary songs (COS+) while in the magnet relative to the control situation, without song stimulation (COS-). Adapted with permission of Tindemans et al.³³

overview of the adult songbird brain showing the song control nuclei and their connections in the telencephalon. Two major neuronal pathways exist, originating from distinct cell populations within the high vocal center (HVC), that project to area X or to the nucleus robustus archistriatalis (RA). MEMRI obtained 6 h following injection of 200 nl of an 80-mM solution of MnCl_2 into the HVC clearly shows the HVC, area X, and area RA (figure 3).³⁰ Using MEMRI, significant seasonal differences in the volume, amount of Mn^{2+} uptake, and rate of transport in the song control nuclei between males and females were observed.³⁰ In addition, changes in the song control nuclei in response to exposure to conspecific songs (figure 3),³³ to steroid treatment,³⁴ or to seasonal changes in song output⁷¹ shows that both functional and morphological changes in the brain associated with behavior can be followed longitudinally with MEMRI.

MEMRI of Cerebral Function

A promising use of MEMRI is to map functional brain activity. This is possible because one of the major means of entry of Mn^{2+} into cells is through voltage-gated cal-

cium channels,^{72–74} meaning it can accumulate in excitable cells such as neurons and astrocytes in an activity-dependent manner. Indeed, brain activity in rodents has been successfully probed with MEMRI.^{39–42,45,46,75,76} In these studies, MnCl_2 was infused into the bloodstream, while the brain was stimulated pharmacologically or with a sensory stimulation paradigm. Local increased brain activity led to an increased Mn^{2+} influx and thus to increased contrast on T_1 -weighted MRI. Functional maps produced with MEMRI have the advantage of being based on calcium influx, rather than on cerebral hemodynamics. Therefore, they show better spatial localization than functional maps produced by conventional fMRI methods.⁴⁰ However, a significant problem for detection of functional activation with MEMRI is the fact that brain electrical activity is strongly dependent on the anesthetic depth. Deep anesthesia significantly suppresses activity, making it difficult to detect signal changes. Light anesthesia, on the other hand, may induce stimulus unrelated or spatially unspecific activation. In order to control for the anesthetic depth, a dynamic MEMRI technique was proposed to reduce nonspecific signals associated with light anesthesia.⁴¹

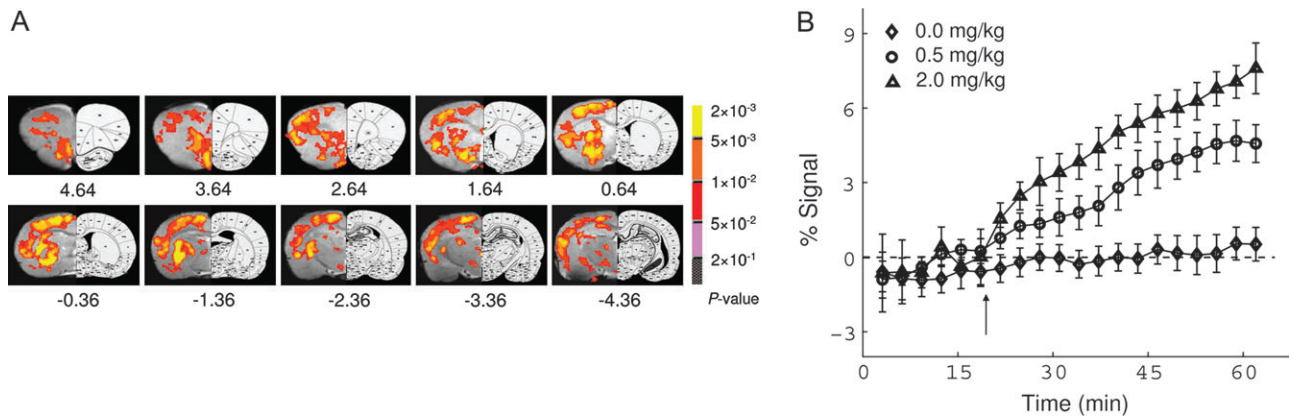


Fig. 4. (A) MEMRI of acute cocaine-induced brain activation. Activation maps are superimposed onto T_2 -weighted MRI with corresponding rat brain atlas sections shown on the right. Activated voxels are clustered in the hemisphere with the BBB disrupted by hyperosmolar mannitol. The contralateral hemisphere had an intact BBB and did not show activation. Activated structures include olfactory cortex; medial, ventral, and lateral orbital cortex; pre-limbic cortex; cingulate cortex; nucleus accumbens (NAc), caudate putamen; ventral pallidus; external globus pallidus; agranular insular cortex; thalamus; hypothalamus; retrosplenial dysgranular cortex; hippocampus; and primary and secondary somatosensory and motor cortex. (B) Averaged MEMRI response time course in the NAc from animals receiving saline ($n = 6$) and 0.5 mg/kg ($n = 5$) and 2.0 mg/kg ($n = 6$) cocaine. All time courses were normalized to the baseline signal after bolus injection of mannitol, but before the injection of cocaine or saline. Adapted with permission of Lu et al.⁴⁶

This technique relies on acquisition of a baseline “resting” activity signal during infusion of Mn^{2+} , but before presentation of the stimulus, to probe for quiescent rates of Mn^{2+} enhancement unrelated to the intended stimulus paradigm.⁴¹

In order to get sufficient accumulation of Mn^{2+} in the active regions of the cerebral cortex, it is necessary to open the BBB. This is because the cortex is located remotely from the major ventricular bodies in the brain, where transport of manganese is highest, as mentioned above. Disruption of the BBB is usually done with a highly concentrated ($\sim 25\%$) solution of D-mannitol, a hypertonic agent that causes temporary and reversible breakage⁷⁷ (for example, see figure 4). After BBB disruption and upon brain stimulation, Mn^{2+} accumulates in active regions on a short time scale (minutes), but like in the case of systemic administration, once accumulated it does not leave the regions for several hours. The difference in Mn^{2+} influx and efflux rates offers the advantage of allowing Mn^{2+} to be delivered outside the MRI, while the animal is being stimulated or behaving in complex environments.³⁹ A disadvantage, however, is that rapid changes in activity, and in particular, deactivation, cannot readily be followed with MEMRI. While the BBB imposes a significant limitation to the delivery of Mn^{2+} to the cortex, regions of the brain situated adjacent to the main ventricles can be studied without the need to disrupt the BBB. This is the case of the hypothalamus, an endocrine organ in the CNS that is responsible, along with the Pit, for regulation of several aspects of the energy homeostasis system, such as appetite and maintenance of stable osmotic pressure in blood vessels and other extracellular compartments.⁴³ Recently, a few functional studies in the hypothalamus have been successfully performed

in the rodent brain without the need to disrupt the BBB.^{43,78–80} Finally, our studies in the marmoset have shown that large accumulations of manganese can be achieved in the nonhuman primate visual cortex, which offers another opportunity for functional MEMRI without breaking the BBB.²⁶

MEMRI in Translational Models of Brain Disease

Because of the dependence of the rate of uptake of Mn^{2+} on rates of intracellular calcium influx, Mn^{2+} serves as a reliable marker of normal tissue function. Abnormal brain function associated with pathological conditions entail abnormal rates of Mn^{2+} uptake, which are amenable to detection by MEMRI. Therefore, MEMRI is increasingly utilized in translational models of brain disease. For example, MEMRI has been used to detect episodes of anoxic depolarization associated with stroke^{75,81} and cortical spreading depression.⁸² More recently, MEMRI has been used to study the functional reorganization of the rodent cortex following unilateral occlusion of the middle cerebral artery,^{83,84} providing significant insights into the mechanisms underlying functional loss and recovery after stroke. Other translational models of brain disease, including Parkinson’s disease,⁸⁵ Alzheimer’s disease,^{37,86} and epilepsy,^{87–90} are being increasingly investigated with MEMRI. These studies are largely based on quantification of the rate of Mn^{2+} uptake as well as the relative intensity of MEMRI signal enhancement as markers of the functional activity of the specific brain regions involved in the disease model. Manganese also has extensive applications in the study of brain tumors,^{91,92} where the strong uptake of Mn^{2+} by

the tumor is used to define tumor volume and aid in the evaluation of therapeutic efforts.

Other applications of MEMRI in translational research include its use to study spinal cord injury,^{93–95} in which the tract-tracing properties of manganese combine well with its functional properties to allow assessment of connectivity, direction and rate of transport, as well as the functional improvement associated with healing and therapy strategies.^{96–98} The same applies to the study of translational models of cerebral palsy,^{99–101} in which a hypoxic-ischemic lesion of the cortex is created either in the pre- or the postnatal period. Finally, translational functional models of chemical dependency exist in which the functional brain response to administration of cocaine⁴⁶ (figure 4) or methamphetamine,¹⁰² and MEMRI detects changes in the functional brain regions and in the neuronal pathways associated with the psychostimulants.

All the above examples of the use of MEMRI in translational brain research point out to the usefulness and versatility of the technique in probing the anatomical, functional, and structural features of the most diverse models of brain pathology, which can be used to define and evaluate therapeutic strategies that may have a promising impact in the improvement of human health care.

Challenges for MEMRI

A few challenges stand ahead of taking full advantage of all the benefits MEMRI has to offer. First and foremost, in order for manganese to become a useful contrast agent in radiology, neurology, and psychiatry, a method of minimizing its neurotoxicity in humans must be discovered. This requires using as low a dose as possible, which limits the detectability by MRI, an inherently insensitive imaging modality. In addition, further development of manganese-based MRI contrast agents should be pursued. There is currently one agent, Mn-dipyridoxyl-diphosphate (MnDPDP, or TeslascanTM, Mangafodipir, manufactured by GE Healthcare), which is currently used in human clinical imaging of the liver.¹⁰³ Associated with the use of as small amounts of Mn²⁺ as possible is the need to develop and further refine MRI pulse sequences that are sensitive to very small changes in the water relaxation rates.¹⁰⁴ While the doses of Mn²⁺ presently used in animals are too high for use in humans, subtle features of the brain neuroarchitecture, such as cortical layers, need even higher doses to produce adequate image contrast for detection. Concomitant to improvements in the sensitivity of MEMRI techniques, it is equally important to develop new ways to administer MnCl₂ directly to the target organ of interest without having to go to other vital organs, such as the heart, the liver, and the kidneys during a systemic administration. For example, the use of direct, intrathecal,¹⁰⁵ or intraventricular¹⁰⁶ administration of MnCl₂ is a feasible way to deliver large amounts of

MnCl₂ to the brain without the complications of a large systemic dose. As well, the use of a continuous infusion via a cannula implanted directly in the region of interest accomplishes efficient delivery of Mn²⁺ for tract-tracing purposes.³⁸

Second, further work is necessary to understand the biology and the dynamics of Mn²⁺ at all levels of the body. It is essential to better understand the transport and lifetime of manganese in the bloodstream to maximize its availability for uptake by the brain. The transport of Mn²⁺ across the BBB and across the choroid plexus needs further investigation, as this determines the final contrast in the brain. It is equally important to understand exactly how Mn²⁺ enters the cells to turn MEMRI into a quantitative index of calcium influx.

Finally, as disruption in manganese homeostasis may be itself related to a few specific brain disorders, such as Parkinson's disease¹⁰⁷ or schizophrenia,^{108–111} careful planning of the experiments to use MEMRI in translational models of such disorders are necessary to avoid possible confounds that may complicate interpretation of the results and misguide future research.

There is no doubt that the combination of the rich biology of Mn²⁺ and its properties as an MRI contrast agent allow MEMRI to be a uniquely useful and versatile technique in modern neuroimaging. Indeed, there are presently 3 major ways to use MEMRI. First, simple systemic administration of Mn²⁺ leads to detection of anatomical structures that would otherwise be difficult to reveal. Second, Mn²⁺ is stored and transported in axonal tracts and is released in the synaptic clefts, becoming available for uptake by the next neuron in a way that enables trans-synaptic tracing of neuronal pathways. Third, the dynamics of Mn²⁺ entry into excitable cells in the CNS is intrinsically linked to activity of voltage-gated calcium channels, allowing MEMRI to map functional brain regions. The combination of all the above properties leads to ample opportunities to use MEMRI for studying translational models of brain disease. It is difficult to think of another neuroimaging technique with such a broad range of applications and versatility.

Funding

Intramural Research Program of the National Institute of Neurological Disorders and Stroke, National Institutes of Health (Alan P. Koretsky, Scientific Director).

References

1. Jasanoff A. MRI contrast agents for functional molecular imaging of brain activity. *Curr Opin Neurobiol.* 2007; 17(5):593–600.
2. Li Y, Huang TT, Carlson EJ, et al. Dilated cardiomyopathy and neonatal lethality in mutant mice lacking manganese superoxide dismutase. *Nat Genet.* 1995;11(4):376–381.

3. Gunter TE, Gavin CE, Aschner M, Gunter KK. Speciation of manganese in cells and mitochondria: a search for the proximal cause of manganese neurotoxicity. *Neurotoxicology*. 2006;27(5):765–776.
4. Zwingmann C, Leibfritz D, Hazell AS. Brain energy metabolism in a sub-acute rat model of manganese neurotoxicity: an ex vivo nuclear magnetic resonance study using [1-13C]glucose. *Neurotoxicology*. 2004;25(4):573–587.
5. Wedler FC, Denman RB. Glutamine synthetase: the major Mn(II) enzyme in mammalian brain. *Curr Top Cell Regul*. 1984;24:153–169.
6. Crossgrove J, Zheng W. Manganese toxicity upon overexposure. *NMR Biomed*. 2004;17(8):544–553.
7. Aschner JL, Aschner M. Nutritional aspects of manganese homeostasis. *Mol Aspects Med*. 2005;26(4–5):353–362.
8. Aschner M, Dorman DC. Manganese: pharmacokinetics and molecular mechanisms of brain uptake. *Toxicol Rev*. 2006;25(3):147–154.
9. Aschner M, Guilarte TR, Schneider JS, Zheng W. Manganese: recent advances in understanding its transport and neurotoxicity. *Toxicol Appl Pharmacol*. 2007;221(2):131–147.
10. Takeda A. Manganese action in brain function. *Brain Res Brain Res Rev*. 2003;41(1):79–87.
11. Sloot WN, Gramsbergen JB. Axonal transport of manganese and its relevance to selective neurotoxicity in the rat basal ganglia. *Brain Res*. 1994;657(1–2):124–132.
12. Takeda A, Kodama Y, Ishiwatari S, Okada S. Manganese transport in the neural circuit of rat CNS. *Brain Res Bull*. 1998;45(2):149–152.
13. Takeda A, Ishiwatari S, Okada S. In vivo stimulation-induced release of manganese in rat amygdala. *Brain Res*. 1998;811(1–2):147–151.
14. Takeda A, Sotogaku N, Oku N. Manganese influences the levels of neurotransmitters in synapses in rat brain. *Neuroscience*. 2002;114(3):669–674.
15. Lee JH, Koretsky AP. Manganese enhanced magnetic resonance imaging. *Curr Pharm Biotechnol*. 2004;5(6):529–537.
16. Koretsky AP, Silva AC. Manganese-enhanced magnetic resonance imaging (MEMRI). *NMR Biomed*. 2004;17(8):527–531.
17. Pautler RG. Biological applications of manganese-enhanced magnetic resonance imaging. *Methods Mol Med*. 2006;124:365–386.
18. Bock NA, Silva AC. Manganese: a unique neuroimaging contrast agent. *Future Neurology*. 2007;2(3):297–395.
19. Natt O, Watanabe T, Boretius S, Radulovic J, Frahm J, Michaelis T. High-resolution 3D MRI of mouse brain reveals small cerebral structures in vivo. *J Neurosci Methods*. 2002;120(2):203–209.
20. Watanabe T, Natt O, Boretius S, Frahm J, Michaelis T. In vivo 3D MRI staining of mouse brain after subcutaneous application of MnCl₂. *Magn Reson Med*. 2002;48(5):852–859.
21. Watanabe T, Radulovic J, Spiess J, et al. In vivo 3D MRI staining of the mouse hippocampal system using intracerebral injection of MnCl₂. *Neuroimage*. 2004;22(2):860–867.
22. Aoki I, Wu YJ, Silva AC, Lynch RM, Koretsky AP. In vivo detection of neuroarchitecture in the rodent brain using manganese-enhanced MRI. *Neuroimage*. 2004;22(3):1046–1059.
23. Watanabe T, Radulovic J, Boretius S, Frahm J, Michaelis T. Mapping of the habenulo-interpeduncular pathway in living mice using manganese-enhanced 3D MRI. *Magn Reson Imaging*. 2006;24(3):209–215.
24. Bock NA, Paiva FF, Silva AC. Fractionated manganese-enhanced MRI. *NMR Biomed*. October 14, 2007.
25. Silva AC, Lee JH, Wu CW, et al. Detection of cortical laminar architecture using manganese-enhanced MRI. *J Neurosci Methods STAT- In-Data-Review*. 2008;2:246–257.
26. Bock NA, Paiva FF, Nascimento GC, Newman JD, Silva AC. Cerebrospinal fluid to brain transport of manganese in a non-human primate revealed by MRI. *Brain Res*. 2008;1198:160–170.
27. Pautler RG, Silva AC, Koretsky AP. In vivo neuronal tract tracing using manganese-enhanced magnetic resonance imaging. *Magn Reson Med*. 1998;40(5):740–748.
28. Watanabe T, Michaelis T, Frahm J. Mapping of retinal projections in the living rat using high-resolution 3D gradient-echo MRI with Mn²⁺-induced contrast. *Magn Reson Med*. 2001;46(3):424–429.
29. Pautler RG, Koretsky AP. Tracing odor-induced activation in the olfactory bulbs of mice using manganese-enhanced magnetic resonance imaging. *Neuroimage*. 2002;16(2):441–448.
30. Van der LA, Verhoye M, Van M, et al. In vivo manganese-enhanced magnetic resonance imaging reveals connections and functional properties of the songbird vocal control system. *Neuroscience*. 2002;112(2):467–474.
31. Saleem KS, Pauls JM, Augath M, et al. Magnetic resonance imaging of neuronal connections in the macaque monkey. *Neuron*. 2002;34(5):685–700.
32. Pautler RG, Mongeau R, Jacobs RE. In vivo trans-synaptic tract tracing from the murine striatum and amygdala utilizing manganese enhanced MRI (MEMRI). *Magn Reson Med*. 2003;50(1):33–39.
33. Tindemans I, Verhoye M, Balthazart J, Van der LA. In vivo dynamic ME-MRI reveals differential functional responses of RA- and area X-projecting neurons in the HVC of canaries exposed to conspecific song. *Eur J Neurosci*. 2003;18(12):3352–3360.
34. Van Meir V, Verhoye M, Absil P, Eens M, Balthazart J, Van der LA. Differential effects of testosterone on neuronal populations and their connections in a sensorimotor brain nucleus controlling song production in songbirds: a manganese enhanced-magnetic resonance imaging study. *Neuroimage*. 2004;21(3):914–923.
35. Tindemans I, Boumans T, Verhoye M, Van der Linden A. IR-SE and IR-MEMRI allow in vivo visualization of oscine neuroarchitecture including the main forebrain regions of the song control system. *NMR Biomed*. 2006;19(1):18–29.
36. Murayama Y, Weber B, Saleem KS, Augath M, Logothetis NK. Tracing neural circuits in vivo with Mn-enhanced MRI. *Magn Reson Imaging*. 2006;24(4):349–358.
37. Smith KD, Kallhoff V, Zheng H, Pautler RG. In vivo axonal transport rates decrease in a mouse model of Alzheimer's disease. *Neuroimage*. 2007;35(4):1401–1408.
38. Canals S, Beyerlein M, Keller AL, Murayama Y, Logothetis NK. Magnetic resonance imaging of cortical connectivity in vivo. *Neuroimage*. 2008;40(2):458–472.
39. Lin YJ. MRI of the rat and mouse brain after systemic administration of MnCl₂ [dissertation]. Pittsburgh: Carnegie Mellon University; 1997.
40. Duong TQ, Silva AC, Lee SP, Kim SG. Functional MRI of calcium-dependent synaptic activity: cross correlation with CBF and BOLD measurements. *Magn Reson Med*. 2000;43(3):383–392.
41. Aoki I, Tanaka C, Takegami T, et al. Dynamic activity-induced manganese-dependent contrast magnetic resonance

- imaging (DAIM MRI). *Magn Reson Med.* 2002;48(6):927–933.
42. Yu X, Wadghiri YZ, Sanes DH, Turnbull DH. In vivo auditory brain mapping in mice with Mn-enhanced MRI. *Nat Neurosci.* 2005;8(7):961–968.
 43. Kuo YT, Herlihy AH, So PW, Bell JD. Manganese-enhanced magnetic resonance imaging (MEMRI) without compromise of the blood-brain barrier detects hypothalamic neuronal activity in vivo. *NMR Biomed.* 2006;19(8):1028–1034.
 44. Yu X, Sanes DH, Aristizabal O, Wadghiri YZ, Turnbull DH. Large-scale reorganization of the tonotopic map in mouse auditory midbrain revealed by MRI. *Proc Natl Acad Sci USA.* 2007;104(29):12193–12198.
 45. Weng JC, Chen JH, Yang PF, Tseng WY. Functional mapping of rat barrel activation following whisker stimulation using activity-induced manganese-dependent contrast. *Neuroimage.* 2007;36(4):1179–1188.
 46. Lu H, Xi ZX, Gitajn L, Rea W, Yang Y, Stein EA. Cocaine-induced brain activation detected by dynamic manganese-enhanced magnetic resonance imaging (MEMRI). *Proc Natl Acad Sci USA.* 2007;104(7):2489–2494.
 47. Yu X, Zou J, Babb JS, Johnson G, Sanes DH, Turnbull DH. Statistical mapping of sound-evoked activity in the mouse auditory midbrain using Mn-enhanced MRI. *Neuroimage.* 2008;39(1):223–230.
 48. Dobson AW, Erikson KM, Aschner M. Manganese neurotoxicity. *Ann N Y Acad Sci.* 2004;1012:115–128.
 49. Racette BA, Antenor JA, McGee-Minnich L, et al. [18F]FDOPA PET and clinical features in parkinsonism due to manganese. *Mov Disord.* 2005;20(4):492–496.
 50. Chandra SV, Shukla GS. Role of iron deficiency in inducing susceptibility to manganese toxicity. *Arch Toxicol.* 1976;35(4):319–323.
 51. Wolf GL, Baum L. Cardiovascular toxicity and tissue proton T1 response to manganese injection in the dog and rabbit. *AJR Am J Roentgenol.* 1983;141(1):193–197.
 52. Silva AC, Lee JH, Aoki I, Koretsky AP. Manganese-enhanced magnetic resonance imaging (MEMRI): methodological and practical considerations. *NMR Biomed.* 2004;17(8):532–543.
 53. Kuo YT, Herlihy AH, So PW, Bhakoo KK, Bell JD. In vivo measurements of T1 relaxation times in mouse brain associated with different modes of systemic administration of manganese chloride. *J Magn Reson Imaging.* 2005;21(4):334–339.
 54. Lee JH, Silva AC, Merkle H, Koretsky AP. Manganese-enhanced magnetic resonance imaging of mouse brain after systemic administration of MnCl₂: dose-dependent and temporal evolution of T1 contrast. *Magn Reson Med.* 2005;53(3):640–648.
 55. Takeda A, Sawashita J, Okada S. Biological half-lives of zinc and manganese in rat brain. *Brain Res.* 1995;695(1):53–58.
 56. Zhang S, Zhou Z, Fu J. Effect of manganese chloride exposure on liver and brain mitochondria function in rats. *Environ Res.* 2003;93(2):149–157.
 57. Jelsing J, Hay-Schmidt A, Dyrby T, Hemmingsen R, Uyllings HB, Pakkenberg B. The prefrontal cortex in the Gottingen minipig brain defined by neural projection criteria and cytoarchitecture. *Brain Res Bull.* 2006;70(4–6):322–336.
 58. Watanabe T, Frahm J, Michaelis T. Functional mapping of neural pathways in rodent brain in vivo using manganese-enhanced three-dimensional magnetic resonance imaging. *NMR Biomed.* 2004;17(8):554–568.
 59. Watanabe T, Schachtner J, Krizan M, Boretius S, Frahm J, Michaelis T. Manganese-enhanced 3D MRI of established and disrupted synaptic activity in the developing insect brain in vivo. *J Neurosci Methods.* 2006;158(1):50–55.
 60. Angenstein F, Niessen HG, Goldschmidt J, et al. Manganese-enhanced MRI reveals structural and functional changes in the cortex of Bassoon mutant mice. *Cereb Cortex.* 2007;17(1):28–36.
 61. Murphy VA, Wadhvani KC, Smith QR, Rapoport SI. Saturable transport of manganese(II) across the rat blood-brain barrier. *J Neurochem.* 1991;57(3):948–954.
 62. Rabin O, Hegedus L, Bourre JM, Smith QR. Rapid brain uptake of manganese(II) across the blood-brain barrier. *J Neurochem.* 1993;61(2):509–517.
 63. Wadghiri YZ, Blind JA, Duan X, et al. Manganese-enhanced magnetic resonance imaging (MEMRI) of mouse brain development. *NMR Biomed.* 2004;17(8):613–619.
 64. de Sousa PL, de Souza SL, Silva AC, de Souza RE, de Castro RM. Manganese-enhanced magnetic resonance imaging (MEMRI) of rat brain after systemic administration of MnCl₂: changes in T1 relaxation times during postnatal development. *J Magn Reson Imaging.* 2007;25(1):32–38.
 65. Jiang Y, Zheng W, Long L, et al. Brain magnetic resonance imaging and manganese concentrations in red blood cells of smelting workers: search for biomarkers of manganese exposure. *Neurotoxicology.* 2006;28(1):126–135.
 66. Thuen M, Singstad TE, Pedersen TB, et al. Manganese-enhanced MRI of the optic visual pathway and optic nerve injury in adult rats. *J Magn Reson Imaging.* 2005;22(4):492–500.
 67. Lindsey JD, Scadeng M, Dubowitz DJ, Crowston JG, Weinreb RN. Magnetic resonance imaging of the visual system in vivo: transsynaptic illumination of V1 and V2 visual cortex. *Neuroimage.* 2007;34(4):1619–1626.
 68. Allegrini PR, Wiessner C. Three-dimensional MRI of cerebral projections in rat brain in vivo after intracortical injection of MnCl₂. *NMR Biomed.* 2003;16(5):252–256.
 69. Lee JW, Park JA, Lee JJ, et al. Manganese-enhanced auditory tract-tracing MRI with cochlear injection. *Magn Reson Imaging.* 2007;25(5):652–656.
 70. Van der LA, Van MV, Tindemans I, Verhoye M, Balthazart J. Applications of manganese-enhanced magnetic resonance imaging (MEMRI) to image brain plasticity in song birds. *NMR Biomed.* 2004;17(8):602–612.
 71. Van Meir V, Pavlova D, Verhoye M, et al. In vivo MR imaging of the seasonal volumetric and functional plasticity of song control nuclei in relation to song output in a female songbird. *Neuroimage.* 2006;31(3):981–992.
 72. Drapeau P, Nachshen DA. Manganese fluxes and manganese-dependent neurotransmitter release in presynaptic nerve endings isolated from rat brain. *J Physiol.* 1984;348:493–510.
 73. Narita K, Kawasaki F, Kita H. Mn and Mg influxes through Ca channels of motor nerve terminals are prevented by verapamil in frogs. *Brain Res.* 1990;510(2):289–295.
 74. Hunter DR, Haworth RA, Berkoff HA. Cellular manganese uptake by the isolated perfused rat heart: a probe for the sarcolemma calcium channel. *J Mol Cell Cardiol.* 1981;13(9):823–832.
 75. Aoki I, Ebisu T, Tanaka C, et al. Detection of the anoxic depolarization of focal ischemia using manganese-enhanced MRI. *Magn Reson Med.* 2003;50(1):7–12.
 76. Brozoski TJ, Ciobanu L, Bauer CA. Central neural activity in rats with tinnitus evaluated with manganese-enhanced magnetic resonance imaging (MEMRI). *Hear Res.* 2007;228(1–2):168–179.

77. Neuwelt EA, Frenkel EP, Diehl JT, et al. Osmotic blood-brain barrier disruption: a new means of increasing chemotherapeutic agent delivery. *Trans Am Neurol Assoc.* 1979;104:256–260.
78. Chaudhri OB, Parkinson JR, Kuo YT, et al. Differential hypothalamic neuronal activation following peripheral injection of GLP-1 and oxyntomodulin in mice detected by manganese-enhanced magnetic resonance imaging. *Biochem Biophys Res Commun.* 2006;350(2):298–306.
79. Kuo YT, Parkinson JR, Chaudhri OB, et al. The temporal sequence of gut peptide CNS interactions tracked in vivo by magnetic resonance imaging. *J Neurosci.* 2007;27(45):12341–12348.
80. So PW, Yu WS, Kuo YT, et al. Impact of resistant starch on body fat patterning and central appetite regulation. *PLoS ONE.* 2007;2(12):e1309.
81. Aoki I, Naruse S, Tanaka C. Manganese-enhanced magnetic resonance imaging (MEMRI) of brain activity and applications to early detection of brain ischemia. *NMR Biomed.* 2004;17(8):569–580.
82. Henning EC, Meng X, Fisher M, Sotak CH. Visualization of cortical spreading depression using manganese-enhanced magnetic resonance imaging. *Magn Reson Med.* 2005;53(4):851–857.
83. van der Zijden JP, Wu O, van der TA, Roeling TP, Bleys RL, Dijkhuizen RM. Changes in neuronal connectivity after stroke in rats as studied by serial manganese-enhanced MRI. *Neuroimage.* 2007;34(4):1650–1657.
84. van der Zijden JP, Bouts MJ, Wu O, et al. Manganese-enhanced MRI of brain plasticity in relation to functional recovery after experimental stroke. *J Cereb Blood Flow Metab.* 2008;28(4):832–840.
85. Pelled G, Bergman H, Ben-Hur T, Goelman G. Manganese-enhanced MRI in a rat model of Parkinson's disease. *J Magn Reson Imaging.* 2007;26(4):863–870.
86. Benveniste H, Ma Y, Dhawan J, et al. Anatomical and functional phenotyping of mice models of Alzheimer's disease by MR microscopy. *Ann N Y Acad Sci.* 2007;1097:12–29.
87. Hsu YH, Lee WT, Chang C. Multiparametric MRI evaluation of kainic acid-induced neuronal activation in rat hippocampus. *Brain.* 2007;130(Pt 12):3124–3134.
88. Alvestad S, Goa PE, Qu H, et al. In vivo mapping of temporospatial changes in manganese enhancement in rat brain during epileptogenesis. *Neuroimage.* 2007;38(1):57–66.
89. Obenaus A, Jacobs RE. Magnetic resonance imaging of functional anatomy: use for small animal epilepsy models. *Epilepsia.* 2007;48:Suppl. 411–17.
90. Immonen RJ, Kharatishvili I, Sierra A, Einula C, Pitkanen A, Grohn OH. Manganese enhanced MRI detects mossy fiber sprouting rather than neurodegeneration, gliosis or seizure-activity in the epileptic rat hippocampus. *Neuroimage.* 2008;40(4):1718–1730.
91. Cross DJ, Flexman JA, Anzai Y, et al. In vivo manganese MR imaging of calcium influx in spontaneous rat pituitary adenoma. *AJNR Am J Neuroradiol.* 2007;28(10):1865–1871.
92. Hegedus B, Banerjee D, Yeh TH, et al. Preclinical cancer therapy in a mouse model of neurofibromatosis-1 optic glioma. *Cancer Res.* 2008;68(5):1520–1528.
93. Bilgen M, Dancause N, Al-Hafez B, He YY, Malone TM. Manganese-enhanced MRI of rat spinal cord injury. *Magn Reson Imaging.* 2005;23(7):829–832.
94. Bilgen M, Peng W, Al-Hafez B, Dancause N, He YY, Cheney PD. Electrical stimulation of cortex improves corticospinal tract tracing in rat spinal cord using manganese-enhanced MRI. *J Neurosci Methods.* 2006;156(1–2):17–22.
95. Bilgen M. Imaging corticospinal tract connectivity in injured rat spinal cord using manganese-enhanced MRI. *BMC Med Imaging.* 2006;6:15.
96. Stieltjes B, Klussmann S, Bock M, et al. Manganese-enhanced magnetic resonance imaging for in vivo assessment of damage and functional improvement following spinal cord injury in mice. *Magn Reson Med.* 2006;55(5):1124–1131.
97. Bonny JM, Mailly P, Renou JP, Orsal D, Benmoussa A, Stettler O. Analysis of laminar activity in normal and injured rat spinal cord by manganese enhanced MRI. *Neuroimage.* 2008;40(4):154–155.
98. Walder N, Petter-Puchner AH, Brejnikow M, Redl H, Essig M, Stieltjes B. Manganese enhanced magnetic resonance imaging in a contusion model of spinal cord injury in rats: correlation with motor function. *Invest Radiol.* 2008;43(5):277–283.
99. Drobyshevsky A, Robinson AM, Derrick M, et al. Sensory deficits and olfactory system injury detected by novel application of MEMRI in newborn rabbit after antenatal hypoxia-ischemia. *Neuroimage.* 2006;32(3):1106–1112.
100. Yang J, Wu EX. Manganese-enhanced MRI detected the gray matter lesions in the late phase of mild hypoxic-ischemic injury in neonatal rat. *Conf Proc IEEE Eng Med Biol Soc.* 2007;2007:51–54.
101. Yang J, Wu EX. Detection of cortical gray matter lesion in the late phase of mild hypoxic-ischemic injury by manganese-enhanced MRI. *Neuroimage.* 2008;39(2):669–679.
102. Hsu YH, Chen CC, Zechariah A, Yen CC, Yang LC, Chang C. Neuronal dysfunction of a long projecting multisynaptic pathway in response to methamphetamine using manganese-enhanced MRI. *Psychopharmacology (Berl).* 2008;196(4):543–553.
103. Federle MP, Chezmar JL, Rubin DL, et al. Safety and efficacy of mangafodipir trisodium (MnDPDP) injection for hepatic MRI in adults: results of the U.S. multicenter phase III clinical trials (safety). *J Magn Reson Imaging.* 2000;12(1):186–197.
104. Chuang KH, Koretsky A. Improved neuronal tract tracing using manganese enhanced magnetic resonance imaging with fast T(1) mapping. *Magn Reson Med.* 2006;55(3):604–611.
105. Liu CH, D'Arceuil HE, de Crespigny AJ. Direct CSF injection of MnCl(2) for dynamic manganese-enhanced MRI. *Magn Reson Med.* 2004;51(5):978–987.
106. Morita H, Ogino T, Fujiki N, et al. Sequence of forebrain activation induced by intraventricular injection of hypertonic NaCl detected by Mn²⁺ contrasted T1-weighted MRI. *Auton Neurosci.* 2004;113(1–2):43–54.
107. Olanow CW. Manganese-induced parkinsonism and Parkinson's disease. *Ann N Y Acad Sci.* 2004;1012:209–223.
108. Loven DP, James JF, Biggs L, Little KY. Increased manganese-superoxide dismutase activity in postmortem brain from neuroleptic-treated psychotic patients. *Biol Psychiatry.* 1996;40(3):230–232.
109. Parikh V, Khan MM, Mahadik SP. Differential effects of antipsychotics on expression of antioxidant enzymes and membrane lipid peroxidation in rat brain. *J Psychiatr Res.* 2003;37(1):43–51.
110. Yanik M, Vural H, Kocyigit A, et al. Is the arginine-nitric oxide pathway involved in the pathogenesis of schizophrenia? *Neuropsychobiology.* 2003;47(2):61–65.
111. Yanik M, Kocyigit A, Tutkun H, Vural H, Herken H. Plasma manganese, selenium, zinc, copper, and iron concentrations in patients with schizophrenia. *Biol Trace Elem Res.* 2004;98(2):109–117.